# Dynamics and Instabilities of the Shastry-Sutherland Model

Zhentao Wang[1] and Cristian D. Batista[1,2]
[1]Department of Physics and Astronomy, The University of Tennessee, Knoxville, Tennessee 37996, USA
[2]Quantum Condensed Matter Division and Shull-Wollan Center, Oak Ridge National Laboratory, Oak Ridge, Tennessee 37831, USA

(Received 26 February 2018; published 12 June 2018)

We study the excitation spectrum in the dimer phase of the Shastry-Sutherland model by using an unbiased variational method that works in the thermodynamic limit. The method outputs dynamical correlation functions in all possible channels. This output is exploited to identify the order parameters with the highest susceptibility (single or multitriplon condensation in a specific channel) upon approaching a quantum phase transition in the magnetic field versus the $J'/J$ phase diagram. We find four different instabilities: antiferro spin nematic, plaquette spin nematic, stripe magnetic order, and plaquette order, two of which have been reported in previous studies.

DOI: 10.1103/PhysRevLett.120.247201

The Shastry-Sutherland model (SSM) has become a paradigmatic Hamiltonian of frustrated quantum magnetism [1,2] because it includes an exactly solvable ground state [1], very heavy low-energy excitations [3–8], exotic phases obtained upon varying the ratio $J'/J$ between two competing exchange constants [4,7,9–16], and a series of magnetic field induced magnetization plateaux [3,17–31]. Its realization in $SrCu_2(BO_3)_2$ [3,32,33] enabled various experimental studies, including magnetization [32,34–39], specific heat [40], inelastic neutron scattering (NS) [41–47], far-infrared [48], electron spin resonance (ESR) [49,50], Raman scattering [51], and nuclear magnetic resonance (NMR) [37,52,53]. These studies revealed that a finite Dzyaloshinskii-Moriya (DM) interaction [54,55] must be added to the SSM in order to account for several properties of $SrCu_2(BO_3)_2$ [42–44,46,49,50,53,56–60].

Despite the great theoretical efforts devoted to the SSM, the problem is still far from being solved. Perturbative approaches are only applicable in narrow regimes and conventional numerical methods suffer from severe size effects. As a consequence, the nature of the quantum phase diagram has been debated for a long time [4,7,9–16]. It is thus desirable to develop and apply alternative approaches. The infinite projected entangled-pair states (iPEPS) is an example of an alternative approach that works in the thermodynamic limit [16,29,61]. However, it relies heavily on the initial guess of the physical states and it is difficult to extract dynamical responses.

In this Letter, we introduce an *unbiased* variational method to calculate the excitation spectrum and dynamical responses (susceptibilities) of the SSM in the dimer phase [62]. The method works in the thermodynamic limit and it complements alternative approaches like iPEPS. The basic idea was originally introduced to compute the single-hole dispersion of the square lattice $t$-$J$ model [67,68]. The same method was applied to the Shastry-Sutherland lattice $t$-$J$ model [69,70]. Here we exploit this idea to compute dynamical correlators and dominant instabilities. By working in a reduced Hilbert space, which preserves all model symmetries, we obtain low energy excitations classified by quantum numbers. We then predict the character of the neighboring phases by detecting the order parameter with highest susceptibility. Besides confirming the previously reported plaquette order and antiferro spin-nematic phases, we find two new phases; namely, a plaquette spin-nematic phase and stripe magnetic ordering, induced by simultaneously increasing the magnetic field and $J'/J$. In particular, the plaquette spin-nematic phase explains the nature of the two-triplon states (pinwheels) that crystallize at higher field values [29].

We consider the spin-$\frac{1}{2}$ SSM under a magnetic field [1]:

$$\mathcal{H} = J\sum_{\langle ij\rangle} \boldsymbol{S}_i \cdot \boldsymbol{S}_j + J'\sum_{\langle\langle ij\rangle\rangle} \boldsymbol{S}_i \cdot \boldsymbol{S}_j - h\sum_i S_i^z, \qquad (1)$$

where $\langle ij\rangle$ and $\langle\langle ij\rangle\rangle$ denote intradimer and interdimer neighbors. The unit cell has 4 sites (see Fig. 1). The exact ground state for small enough $J'/J$ and $h$ is a direct product of singlet states on all dimers [1]. The elementary excitations of this "dimer phase" are singlet-triplet excitations known as triplons. Triplons are dressed by quantum fluctuations with a magnetic correlation length $\xi$ that increases with $J'/J$. Methods that can account for the spatial extent of these quantum fluctuations should provide a good description of the low-energy excitation spectrum of the dimer phase.

We start the process by creating local excited states $|\varphi_i\rangle$ (e.g., single and two triplons). We then project these representative states into subspaces with fixed momentum $\boldsymbol{k}$,

 

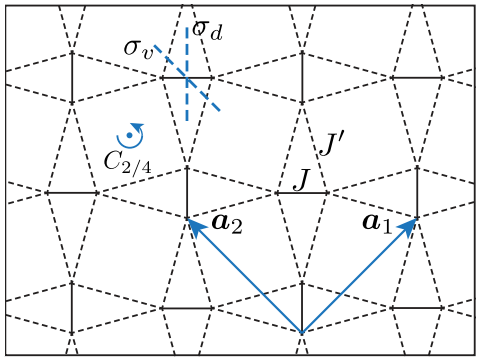


FIG. 1. Lattice structure of the SSM. Intradimer and interdimer exchanges are denoted by $J$ (solid line) and $J'$ (dashed line). The basis of the lattice is labeled by $\{\boldsymbol{a}_1, \boldsymbol{a}_2\}$. The point group operations $\{\sigma_v, \sigma_d, C_2, C_4\}$ are denoted accordingly.

$$|\varphi_i(\boldsymbol{k})\rangle \equiv \frac{\hat{P}_{\boldsymbol{k}}|\varphi_i\rangle}{\sqrt{\langle\varphi_i|\hat{P}_{\boldsymbol{k}}|\varphi_i\rangle}}, \tag{2}$$

where the projector is defined as $\hat{P}_{\boldsymbol{k}} \equiv \frac{1}{N}\sum_{\boldsymbol{r}} e^{i\boldsymbol{k}\cdot\boldsymbol{r}}\hat{T}(\boldsymbol{r})$. $N \to \infty$ (thermodynamic limit) is the total number of unit cells, and $\hat{T}(\boldsymbol{r})$ is the translation operator. Application of $\mathcal{H}$ to $|\varphi_i(\boldsymbol{k})\rangle$ generates new states that dress the corresponding quasiparticle excitation. This procedure can be applied iteratively to systematically improve the variational space. After $M$ iterations, we obtain a basis $\{\varphi_i(\boldsymbol{k})\}$ with good quantum numbers $\boldsymbol{k}$ and $S^z_{\text{tot}}$. The number of iterations determines the spatial range $l$ of the fluctuations that dress the quasiparticle, so the method is then expected to produce accurate results for $l \gtrsim \xi$.

The eigenvalues and eigenvectors of the Hamiltonian restricted to the variational space are obtained by applying the implicitly restarted Arnoldi method [71,72]. The eigenvectors are classified by the Little Group of $C_{4v}$ for each momentum $\boldsymbol{k}$. A continuous phase transition manifests via a vanishing gap (condensation) that signals a phase transition into a broken symmetry state. The symmetry of the new state is determined by the irreducible representation (IREP) of the eigenstate that becomes gapless. To keep the method unbiased, the initial basis must not break the point group symmetry of $\mathcal{H}$ [73].

For illustration, we first focus on the $S^z_{\text{tot}} = 0$ sector relevant to $h = 0$. We include $\mathcal{D} = 14$ $S^z_{\text{tot}} = 0$ initial states to start the iteration [74] and then apply Eq. (1) onto this basis to systematically increase the variational space [76]. After obtaining the lowest energy eigenstates, we use the eigenfunction to calculate $S_{\text{tot}}$ and its IREP [77].

In contrast to the result obtained with perturbative continuous unitary transformations (CUTs) [7], we find that the first instability as a function of $J'/J$ (for $h = 0$) takes place in the $S_{\text{tot}} = 0$ channel with IREP $A_2$ [80]. Figure 2 shows the evolution of the gap as a function of $M$. Convergence is reached beyond $M = 3$ for $J'/J \lesssim 0.5$, but

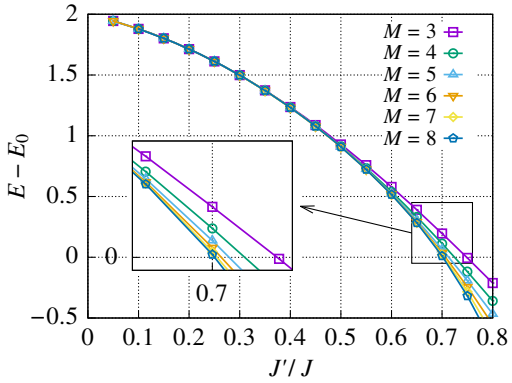


FIG. 2. Gap of the lowest $S_{\text{tot}} = 0, \boldsymbol{k} = (0,0) A_2$ state, at $h = 0$.

the increase of $\xi$ slows down the convergence for larger $J'/J$. Although Eq. (1) does not conserve the triplon number, the state that condenses is adiabatically connected with the corresponding $S_{\text{tot}} = 0$ IREP $A_2$ pure two-triplon state in the $J'/J \to 0$ limit (see Fig. 2).

We can read out the critical value of $J'/J$ when this state condenses. Figure 3(a) shows the evolution of the critical value as we increase $M$ (circles). At $M = 8$, $(J'_c/J)^{(M=8)} \approx 0.702$. Previous tensor network based calculations [15,16] showed that the transition is actually of first order and the transition point is at $J'_c/J = 0.675$ [16]. A susceptibility analysis, like the one presented here, is in general inadequate to detect first order transitions. However, it can still be used to detect the nature of the order parameter if the system still transitions into the broken symmetry state with highest susceptibility [81]. Given that the first-order transition takes place when this susceptibility is still finite, $J'_c/J$ turns out to be smaller than the value at which the susceptibility becomes divergent. This observation explains the difference between the values

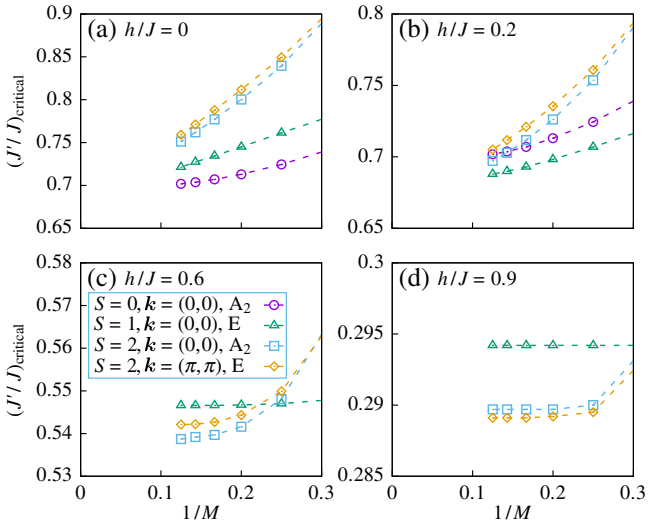


FIG. 3. Critical values of $J'/J$ for the condensation of different states at 4 different magnetic fields.

of $J_c'/J$ obtained with both approaches. In addition, it illustrates their complementary nature. The unbiased susceptibility analysis can be used to detect candidates for broken symmetry states. These candidates can then be tested with biased variational techniques, such as iPEPS, which can produce more accurate values of the transition point.

Since the two-triplon bound state has $S_{\text{tot}} = 0$, the new ground state (condensate) must be nonmagnetic. Furthermore, since the $A_2$ state is odd (even) under reflection (rotation) [74], the new ordered state should only break reflection but not rotation symmetries. These features are consistent with the previously reported plaquette ordering [10,13,15,16]. Figure 4(b) shows a schematic plot of the corresponding bond ordering. As expected, $\langle \boldsymbol{S}_i \cdot \boldsymbol{S}_j \rangle$ becomes different on different plaquettes and there is no magnetic order. In other words, the plaquette order parameter can be defined as $\langle \boldsymbol{S}_i \cdot \boldsymbol{S}_j - \boldsymbol{S}_i \cdot \boldsymbol{S}_{j'} \rangle$, where $ij$ and $ij'$ are two bonds related by a mirror reflection [see Fig. 4(b)].

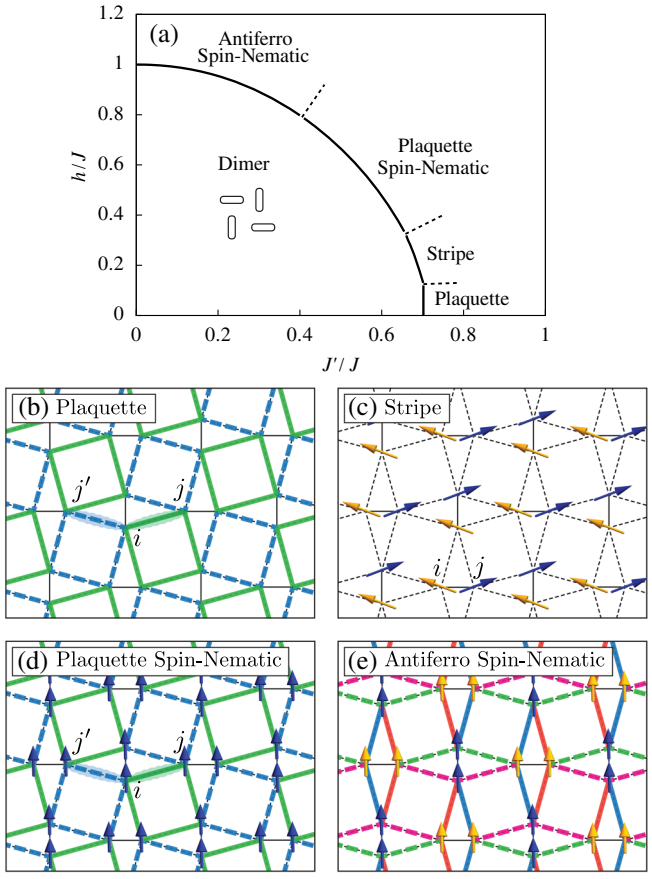


FIG. 4. (a) Phase boundaries between the dimer state and its neighboring phases, obtained from $M = 8$ iterations. (b) Plaquette phase, order parameter defined as $\langle \boldsymbol{S}_i \cdot \boldsymbol{S}_j - \boldsymbol{S}_i \cdot \boldsymbol{S}_{j'} \rangle$. (c) Stripe phase, order parameter defined as $\langle \boldsymbol{S}_i - \boldsymbol{S}_j \rangle$. (d) Plaquette spin-nematic phase, order parameter defined as $\langle S_i^+ S_j^+ - S_i^+ S_{j'}^+ \rangle$. (e) Antiferro spin-nematic phase (bond density wave), bonds with the same line (solid/dashed) but different colors have opposite $\langle S_i^+ S_j^+ \rangle$ while bonds with different lines have different $|\langle S_i^+ S_j^+ \rangle|$.

We consider now the case of nonzero magnetic field. The energy of excited states with finite $S_{\text{tot}}^z$ decreases linearly in $h$. Figure 3(b) shows that the dominant instability for $h/J = 0.2$ corresponds to condensation of a state with $S_{\text{tot}} = 1$, $\boldsymbol{k} = (0, 0)$, and IREP $E$, leading to the stripe magnetic order depicted in Fig. 4(c). The IREP E is a two-dimensional representation corresponding to the two possible directions of the stripes (along $\boldsymbol{a}_1$ or $\boldsymbol{a}_2$). We note that the two same-color spins in the same unit cell are not identical (the corresponding mirror symmetry is broken).

The stripe state has the highest susceptibility over a narrow range $0.66 \lesssim J'/J \lesssim 0.70$ for $M = 8$ iterations [see Fig. 4(a)]. Because of the frustrated exchange interactions, the energies of a few other states are not much higher than the stripe state [74]. Among them, the lowest one is a two-triplon state with $\boldsymbol{k} = (0, 0)$ and IREP $B_1$, corresponding to vector chiral order [82–84]. Although their energies are slightly higher than the stripe magnetic instability within $M \leq 8$, the situation may change in the $M \to \infty$ limit, or if small perturbations are added to the original model.

The $S_{\text{tot}} = 2$ excited states take over for higher magnetic field values. Figure 3(c) shows that for $h/J = 0.6$ the lowest excited state is the $S_{\text{tot}} = 2$ two-triplon bound state with momentum $\boldsymbol{k} = (0, 0)$ and IREP $A_2$. The fact that this state and the $S_{\text{tot}} = 0$ state that condenses at zero field belong to the same point group IREP $A_2$ indicates that the condensation of the $S_{\text{tot}} = 2$ $A_2$ state also leads to "plaquette" ordering [shown in Fig. 4(d)]; the difference being that the $S_{\text{tot}} = 2$ condensate also breaks the U(1) symmetry group of global spin rotations along the field direction, leading to spin-nematic ordering. In other words, the local bond order parameter is $\langle S_i^+ S_j^+ - S_i^+ S_{j'}^+ \rangle$ instead of $\langle \boldsymbol{S}_i \cdot \boldsymbol{S}_j - \boldsymbol{S}_i \cdot \boldsymbol{S}_{j'} \rangle$ ($ij$ and $ij'$ denote two bonds connected by a mirror reflection $\sigma_d$, see Fig. 4).

As indicated in Fig. 4(a), the "plaquette spin-nematic" state covers a wide range $0.40 \lesssim J'/J \lesssim 0.66$. It has been shown in Ref. [29] that the $\frac{1}{8}$ plateau at slightly higher magnetic field values and $J'/J = 0.63$ is induced by crystallization of $S_{\text{tot}}^z = 2$ bound states. A closer scrutiny of the "pinwheel" structure of these bound states shows that they locally preserve rotational symmetries, while breaking reflection symmetries [29]; i.e., they are the same two-triplon bound states that we are finding in the dilute limit.

Moving away from the plaquette spin-nematic phase towards the $J'/J \ll 1$ limit, it is already known from an early perturbative calculation that $S_{\text{tot}} = 2$ two-triplon bound states with $\boldsymbol{k} = (\pi, \pi)$ give the highest susceptibility [19]. This is confirmed by our variational method [see Fig. 3(d)]. Since the two-triplon bound state has momentum $\boldsymbol{k} = (\pi, \pi)$, the corresponding ordered state also breaks translational symmetry. As shown in Fig. 4(e), $\langle S_i^+ S_j^+ \rangle$ changes sign going from one unit cell to its nearest

neighbors. Similar to the case of the stripe ordering (which also comes from condensation of IREP E states), there are two choices for aligning the bonds. We note that the breaking of the $C_4$ lattice rotational symmetry leads to a modulation of $\langle S_i^z \rangle$ that can be detected with NS experiments.

It is worth mentioning that the two spin-nematic states found in this Letter are different from nematic phases discussed in various other contexts [85–88]. The so-called "Ising-nematic" ordering corresponds to (discrete) lattice rotation symmetry breaking. In contrast, "spin-nematic" ordering corresponds to broken spin rotational symmetry. The spin-nematic orderings discussed in this Letter break both the point group symmetry and spin rotation symmetry [89]. In other words, they are *simultaneously* Ising nematic and spin nematic.

The frustrated nature of the SSM makes the calculation of dynamical response a difficult task. To date, the only calculation including multitriplon contributions is the perturbative CUTs, which breaks down for $J'/J \gtrsim 0.63$ [90]. The variational Hilbert space generated by our method thus provides a more reliable access to dynamical responses via the continued fraction method [91].

Near the phase boundaries, we expect the susceptibilities of corresponding order parameters to diverge at $\omega = 0$. Magnetic orderings, such as the stripe phase, are detected by computing the dynamic structure factor (DSF) [74,92]:

$$S^{-+}(\boldsymbol{k},\omega) = 2\pi \sum_{\nu} |\langle \nu | S^{+}_{\boldsymbol{k}} | 0 \rangle|^2 \delta(\omega + E_0 - E_\nu), \quad (3)$$

which is measured with inelastic NS. As shown Fig. 5(b), the lowest peak of $S^{-+}(\boldsymbol{k},\omega)$ approaches $\omega = 0$ near the phase boundary indicating condensation of an $S_{\text{tot}} = 1$ state.

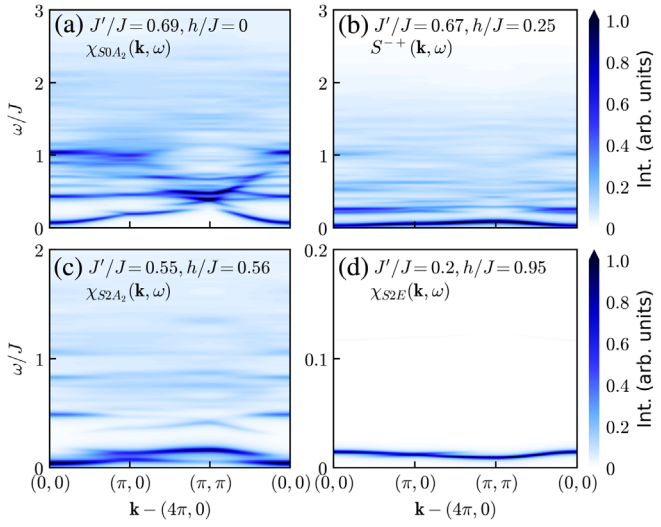


FIG. 5. $T = 0$ DSFs calculated near the phase boundaries at $M = 8$. (a)–(c) Lorentzian broadening factor $\eta = 0.02J$ is used. (d) Lorentzian broadening factor $\eta = 0.001J$ is used.

The divergent susceptibilities of the other phases are revealed by computing two-point dynamical correlation functions of the corresponding order parameters. These order parameters are the operators that create a state that has finite overlap with the one that is condensing. For $J'/J \ll 1$, the lowest energy $S_{\text{tot}} = 2$ eigenstates are known to be a linear combination of triplons located on nearest (and next-nearest) neighbors [19,74]. Denoting the order parameter as $A^{S2E}_{\boldsymbol{k}}$, the corresponding susceptibility is

$$\chi_{S2E}(\boldsymbol{k},\omega) = 2\pi \sum_{\nu} |\langle \nu | A^{S2E}_{\boldsymbol{k}} | 0 \rangle|^2 \delta(\omega + E_0 - E_\nu). \quad (4)$$

Similarly, using the approximate wave functions of the $S_{\text{tot}} = 2\ A_2$ state and the $S_{\text{tot}} = 0\ A_2$ state [74], we can also construct the order parameters and compute the corresponding susceptibilities $\chi_{S2A_2}(\boldsymbol{k},\omega)$ and $\chi_{S0A_2}(\boldsymbol{k},\omega)$. Figure 5 shows the nearly divergent susceptibilities in each channel by picking appropriate Hamiltonian parameters near the phase boundaries.

While the tendency toward stripe ordering can be detected with inelastic NS, the experimental detection of the other phases is nontrivial. Lattice distortions induced by the order parameter through magnetostriction can provide indirect evidence if they are large enough to be detected [82–84]. Experimental knobs, such as pressure, doping, and magnetic field can drive the material into different instabilities [39,47]. Thus, the method presented in this Letter provides valuable insight for revealing the nature of the new phases in such experiments. However, the model relevant to $SrCu_2(BO_3)_2$ also includes DM interactions that modify the single triplon dispersion and can potentially change the phase diagram reported here. In addition, DM interactions reduce the spin rotational symmetry of the model, implying that they can change the nature of the order parameters.

We emphasize that the applicability of the method is not restricted to the SSM considered here. The same method can be used to detect the instabilities of other quantum paramagnets [93]. Especially, it is very difficult to enumerate all the possible instabilities for highly frustrated systems. The low energy spectrum produced by our method provides a valuable educated guess for biased numerical approaches. Given that the method works in the thermodynamic limit, it can also detect incommensurate instabilities, which cannot be handled by most numerical methods.

In summary, we have used an unbiased variational method to study the excitation spectrum of the SSM in the dimer phase. Several instabilities are found next to the dimer phase corresponding to condensations of single-triplon or two-triplon bound states. Two of the instabilities (antiferro spin nematic and plaquette) are known from previous studies and the others (plaquette spin nematic and stripe) are newly discovered in this Letter. The same

method can be used to compute relevant dynamical correlation functions.

We thank S. Haravifard, B. Shastry, G. Ortiz, S. Zhang, and H. Suwa for helpful discussions. Z. W. and C. D. B. are supported by funding from the Lincoln Chair of Excellence in Physics. This work used the Extreme Science and Engineering Discovery Environment (XSEDE) [94] through allocation TG-DMR170029, which is supported by NSF Grant No. ACI-1548562. This research used resources of the Compute and Data Environment for Science (CADES) at the Oak Ridge National Laboratory, which is supported by the Office of Science of the U.S. Department of Energy under Contract No. DE-AC05-00OR22725.

[1] B. S. Shastry and B. Sutherland, Physica (Amsterdam) **108B**, 1069 (1981).
[2] S. Miyahara and K. Ueda, J. Phys. Condens. Matter **15**, R327 (2003).
[3] S. Miyahara and K. Ueda, Phys. Rev. Lett. **82**, 3701 (1999).
[4] Z. Weihong, C. J. Hamer, and J. Oitmaa, Phys. Rev. B **60**, 6608 (1999).
[5] Y. Fukumoto, J. Phys. Soc. Jpn. **69**, 2755 (2000).
[6] C. Knetter, E. Müller-Hartmann, G. S. Uhrig, and E. Müller-Hartmann, J. Phys. Condens. Matter **12**, 9069 (2000).
[7] C. Knetter, A. Bühler, E. Müller-Hartmann, and G. S. Uhrig, Phys. Rev. Lett. **85**, 3958 (2000).
[8] K. Totsuka, S. Miyahara, and K. Ueda, Phys. Rev. Lett. **86**, 520 (2001).
[9] M. Albrecht and F. Mila, Europhys. Lett. **34**, 145 (1996).
[10] A. Koga and N. Kawakami, Phys. Rev. Lett. **84**, 4461 (2000).
[11] A. Koga, J. Phys. Soc. Jpn. **69**, 3509 (2000).
[12] W. Zheng, J. Oitmaa, and C. J. Hamer, Phys. Rev. B **65**, 014408 (2001).
[13] A. Läuchli, S. Wessel, and M. Sigrist, Phys. Rev. B **66**, 014401 (2002).
[14] T. Munehisa and Y. Munehisa, J. Phys. Soc. Jpn. **72**, 160 (2003).
[15] J. Lou, T. Suzuki, K. Harada, and N. Kawashima, arXiv:1212.1999.
[16] P. Corboz and F. Mila, Phys. Rev. B **87**, 115144 (2013).
[17] E. Müller-Hartmann, R. R. P. Singh, C. Knetter, and G. S. Uhrig, Phys. Rev. Lett. **84**, 1808 (2000).
[18] T. Momoi and K. Totsuka, Phys. Rev. B **61**, 3231 (2000).
[19] T. Momoi and K. Totsuka, Phys. Rev. B **62**, 15067 (2000).
[20] Y. Fukumoto and A. Oguchi, J. Phys. Soc. Jpn. **69**, 1286 (2000).
[21] Y. Fukumoto, J. Phys. Soc. Jpn. **70**, 1397 (2001).
[22] G. Misguich, T. Jolicoeur, and S. M. Girvin, Phys. Rev. Lett. **87**, 097203 (2001).
[23] S. Miyahara, F. Becca, and F. Mila, Phys. Rev. B **68**, 024401 (2003).
[24] J. Dorier, K. P. Schmidt, and F. Mila, Phys. Rev. Lett. **101**, 250402 (2008).
[25] A. Abendschein and S. Capponi, Phys. Rev. Lett. **101**, 227201 (2008).
[26] L. Isaev, G. Ortiz, and J. Dukelsky, Phys. Rev. Lett. **103**, 177201 (2009).
[27] M. Takigawa, T. Waki, M. Horvatić, and C. Berthier, J. Phys. Soc. Jpn. **79**, 011005 (2010).
[28] M. Nemec, G. R. Foltin, and K. P. Schmidt, Phys. Rev. B **86**, 174425 (2012).
[29] P. Corboz and F. Mila, Phys. Rev. Lett. **112**, 147203 (2014).
[30] D. A. Schneider, K. Coester, F. Mila, and K. P. Schmidt, Phys. Rev. B **93**, 241107 (2016).
[31] M. Takigawa and F. Mila, in *Introduction to Frustrated Magnetism*, edited by C. Lacroix, P. Mendels, and F. Mila (Springer-Verlag, Berlin, Heidelberg, 2011), Chap. 10, p. 241.
[32] H. Kageyama, K. Yoshimura, R. Stern, N. V. Mushnikov, K. Onizuka, M. Kato, K. Kosuge, C. P. Slichter, T. Goto, and Y. Ueda, Phys. Rev. Lett. **82**, 3168 (1999).
[33] K. Ueda and S. Miyahara, J. Phys. Condens. Matter **11**, L175 (1999).
[34] K. Onizuka, H. Kageyama, Y. Narumi, K. Kindo, Y. Ueda, and T. Goto, J. Phys. Soc. Jpn. **69**, 1016 (2000).
[35] S. E. Sebastian, N. Harrison, P. Sengupta, C. D. Batista, S. Francoual, E. Palm, T. Murphy, N. Marcano, H. A. Dabkowska, and B. D. Gaulin, Proc. Natl. Acad. Sci. U.S.A. **105**, 20157 (2008).
[36] M. Jaime, R. Daou, S. A. Crooker, F. Weickert, A. Uchida, A. E. Feiguin, C. D. Batista, H. A. Dabkowska, and B. D. Gaulin, Proc. Natl. Acad. Sci. U.S.A. **109**, 12404 (2012).
[37] M. Takigawa, M. Horvatić, T. Waki, S. Krämer, C. Berthier, F. Lévy-Bertrand, I. Sheikin, H. Kageyama, Y. Ueda, and F. Mila, Phys. Rev. Lett. **110**, 067210 (2013).
[38] Y. H. Matsuda, N. Abe, S. Takeyama, H. Kageyama, P. Corboz, A. Honecker, S. R. Manmana, G. R. Foltin, K. P. Schmidt, and F. Mila, Phys. Rev. Lett. **111**, 137204 (2013).
[39] S. Haravifard, D. Graf, A. E. Feiguin, C. D. Batista, J. C. Lang, D. M. Silevitch, G. Srajer, B. D. Gaulin, H. A. Dabkowska, and T. F. Rosenbaum, Nat. Commun. **7**, 11956 (2016).
[40] H. Tsujii, C. R. Rotundu, B. Andraka, Y. Takano, H. Kageyama, and Y. Ueda, J. Phys. Soc. Jpn. **80**, 043707 (2011).
[41] H. Kageyama, M. Nishi, N. Aso, K. Onizuka, T. Yosihama, K. Nukui, K. Kodama, K. Kakurai, and Y. Ueda, Phys. Rev. Lett. **84**, 5876 (2000).
[42] O. Cépas, K. Kakurai, L. P. Regnault, T. Ziman, J. P. Boucher, N. Aso, M. Nishi, H. Kageyama, and Y. Ueda, Phys. Rev. Lett. **87**, 167205 (2001).
[43] B. D. Gaulin, S. H. Lee, S. Haravifard, J. P. Castellan, A. J. Berlinsky, H. A. Dabkowska, Y. Qiu, and J. R. D. Copley, Phys. Rev. Lett. **93**, 267202 (2004).
[44] K. Kakurai, K. Nukui, N. Aso, M. Nishi, H. Kadowaki, H. Kageyama, Y. Ueda, L.-P. Regnault, and O. Cépas, Prog. Theor. Phys. Suppl. **159**, 22 (2005).
[45] M. E. Zayed, C. Rüegg, T. Strässle, U. Stuhr, B. Roessli, M. Ay, J. Mesot, P. Link, E. Pomjakushina, M. Stingaciu, K. Conder, and H. M. Rønnow, Phys. Rev. Lett. **113**, 067201 (2014).
[46] P. A. McClarty, F. Krüger, T. Guidi, S. F. Parker, K. Refson, A. W. Parker, D. Prabhakaran, and R. Coldea, Nat. Phys. **13**, 736 (2017).

[47] M. E. Zayed, C. Rüegg, J. Larrea J., A. M. Läuchli, C. Panagopoulos, S. S. Saxena, M. Ellerby, D. F. McMorrow, T. Strässle, S. Klotz, G. Hamel, R. A. Sadykov, V. Pomjakushin, M. Boehm, M. Jiménez-Ruiz, A. Schneidewind, E. Pomjakushina, M. Stingaciu, K. Conder, and H. M. Rønnow, Nat. Phys. **13**, 962 (2017).

[48] T. Rõõm, U. Nagel, E. Lippmaa, H. Kageyama, K. Onizuka, and Y. Ueda, Phys. Rev. B **61**, 14342 (2000).

[49] H. Nojiri, H. Kageyama, K. Onizuka, Y. Ueda, and M. Motokawa, J. Phys. Soc. Jpn. **68**, 2906 (1999).

[50] H. Nojiri, H. Kageyama, Y. Ueda, and M. Motokawa, J. Phys. Soc. Jpn. **72**, 3243 (2003).

[51] P. Lemmens, M. Grove, M. Fischer, G. Güntherodt, V. N. Kotov, H. Kageyama, K. Onizuka, and Y. Ueda, Phys. Rev. Lett. **85**, 2605 (2000).

[52] K. Kodama, M. Takigawa, M. Horvatić, C. Berthier, H. Kageyama, Y. Ueda, S. Miyahara, F. Becca, and F. Mila, Science **298**, 395 (2002).

[53] K. Kodama, S. Miyahara, M. Takigawa, M. Horvatić, C. Berthier, F. Mila, H. Kageyama, and Y. Ueda, J. Phys. Condens. Matter **17**, L61 (2005).

[54] I. Dzyaloshinsky, J. Phys. Chem. Solids **4**, 241 (1958).

[55] T. Moriya, Phys. Rev. **120**, 91 (1960).

[56] S. Miyahara, F. Mila, K. Kodama, M. Takigawa, M. Horvatic, C. Berthier, H. Kageyama, and Y. Ueda, J. Phys. Condens. Matter **16**, S911 (2004).

[57] S. El Shawish, J. Bonča, C. D. Batista, and I. Sega, Phys. Rev. B **71**, 014413 (2005).

[58] Y. F. Cheng, O. Cépas, P. W. Leung, and T. Ziman, Phys. Rev. B **75**, 144422 (2007).

[59] J. Romhányi, K. Totsuka, and K. Penc, Phys. Rev. B **83**, 024413 (2011).

[60] J. Romhányi, K. Penc, and R. Ganesh, Nat. Commun. **6**, 6805 EP (2015).

[61] J. Jordan, R. Orús, G. Vidal, F. Verstraete, and J. I. Cirac, Phys. Rev. Lett. **101**, 250602 (2008).

[62] A numerical method is said to be "variational" when it satisfies the variational principle. Other examples of unbiased variational methods include the density matrix renormalization group [63,64] and matrix product method [65,66], etc.

[63] S. R. White, Phys. Rev. Lett. **69**, 2863 (1992).

[64] S. R. White, Phys. Rev. B **48**, 10345 (1993).

[65] S. Östlund and S. Rommer, Phys. Rev. Lett. **75**, 3537 (1995).

[66] S. Rommer and S. Östlund, Phys. Rev. B **55**, 2164 (1997).

[67] S. A. Trugman, Phys. Rev. B **37**, 1597 (1988).

[68] S. A. Trugman, Phys. Rev. B **41**, 892 (1990).

[69] S. El Shawish and J. Bonča, Phys. Rev. B **74**, 174420 (2006).

[70] S. Haravifard, S. R. Dunsiger, S. El Shawish, B. D. Gaulin, H. A. Dabkowska, M. T. F. Telling, T. G. Perring, and J. Bonča, Phys. Rev. Lett. **97**, 247206 (2006).

[71] C. Lanczos, J. Res. Natl. Bur. Stand. **45**, 255 (1950).

[72] R. B. Lehoucq, D. C. Sorensen, and C. Yang, *ARPACK Users' Guide: Solution of Large-scale Eigenvalue Problems with Implicitly Restarted Arnoldi Methods* (Society for Industrial and Applied Mathematics, Philadelphia, PA, 1998).

[73] This means that the basis generates an invariant subspace of the group. In addition, a fully symmetric initial basis leads to better convergence (as a function of $M$) in comparison with other choices Ref. [69].

[74] See Supplemental Material at http://link.aps.org/supplemental/10.1103/PhysRevLett.120.247201 for the $C_{4v}$ character table, choice of initial basis, construction of the order parameters, dominant instability at zero field, convergence of dynamic structure factors, and the description of a competing chiral state, which includes Ref. [75].

[75] J. P. Elliott and P. G. Dawber, *Symmetry in Physics* (Macmillan Press LTD, London, 1979), Vol. 1.

[76] The computational cost is exponential in the *linear* size of the quasiparticle. In the present case, the dimension of the truncated Hilbert space roughly scales as $\mathcal{D} \propto 6^M \propto 6^l$. For the $S^z_{\mathrm{tot}} = 0$ sector, the dimension of the variational space is $\mathcal{D} = 74$ for $M = 1$, $\mathcal{D} = 396$ for $M = 2$, …, $\mathcal{D} = 17\,730\,330$ for $M = 8$.

[77] In principle, one can switch the order of "diagonalization" and "point group symmetry analysis," to reach larger $M$ and get better convergence. Similar tricks can be found in Refs. [78,79].

[78] V. E. Sinitsyn, I. G. Bostrem, and A. S. Ovchinnikov, J. Phys. A **40**, 645 (2007).

[79] A. M. Läuchli, in *Introduction to Frustrated Magnetism*, edited by C. Lacroix, P. Mendels, and F. Mila (Springer-Verlag, Berlin, Heidelberg, 2011), Chap. 18, p. 481.

[80] The $S = 1$ instability found in Ref. [7] is checked by our method both in $S^z_{\mathrm{tot}} = 0$ and $S^z_{\mathrm{tot}} = 1$ sectors. The energy difference between the two sectors is negligible.

[81] A typical example is the case of attractive interaction between the modes (particles) that become soft. Because of the attraction (negative quartic term in a Ginzburg-Landau expansion) the particle density changes discontinuously (first order transition) before the single-particle excitation becomes gapless.

[82] A. V. Chubukov and O. A. Starykh, Phys. Rev. Lett. **110**, 217210 (2013).

[83] E. Parker and L. Balents, Phys. Rev. B **95**, 104411 (2017).

[84] Z. Wang, A. E. Feiguin, W. Zhu, O. A. Starykh, A. V. Chubukov, and C. D. Batista, Phys. Rev. B **96**, 184409 (2017).

[85] E. Fradkin, S. A. Kivelson, M. J. Lawler, J. P. Eisenstein, and A. P. Mackenzie, Annu. Rev. Condens. Matter Phys. **1**, 153 (2010).

[86] Y. Kamiya, N. Kawashima, and C. D. Batista, Phys. Rev. B **84**, 214429 (2011).

[87] R. M. Fernandes, A. V. Chubukov, J. Knolle, I. Eremin, and J. Schmalian, Phys. Rev. B **85**, 024534 (2012).

[88] R. M. Fernandes, A. V. Chubukov, and J. Schmalian, Nat. Phys. **10**, 97 (2014).

[89] K. Penc and A. M. Läuchli, in *Introduction to Frustrated Magnetism*, edited by C. Lacroix, P. Mendels, and F. Mila (Springer-Verlag, Berlin, Heidelberg, 2011), Chap. 13, p. 331.

[90] C. Knetter and G. S. Uhrig, Phys. Rev. Lett. **92**, 027204 (2004).

[91] E. R. Gagliano and C. A. Balseiro, Phys. Rev. Lett. **59**, 2999 (1987).

[92] According to the fluctuation dissipation theorem, the $T = 0$ dynamic structure factor is equal to the imaginary part of the dynamic susceptibility up to a factor of $-2$.

[93] V. Zapf, M. Jaime, and C. D. Batista, Rev. Mod. Phys. **86**, 563 (2014).

[94] J. Towns, T. Cockerill, M. Dahan, I. Foster, K. Gaither, A. Grimshaw, V. Hazlewood, S. Lathrop, D. Lifka, G. D. Peterson, R. Roskies, J. R. Scott, and N. Wilkens-Diehr, Comput. Sci. Eng. **16**, 62 (2014).